Clim Dyn
DOI 10.1007/s00382-017-3616-y

Identifying a key physical factor sensitive to the performance of Madden–Julian oscillation simulation in climate models

Go-Un Kim[1] · **Kyong-Hwan Seo**[1]

Received: 23 July 2016 / Accepted: 1 March 2017

Abstract A key physical factor in regulating the performance of Madden–Julian oscillation (MJO) simulation is examined by using 26 climate model simulations from the World Meteorological Organization's Working Group for Numerical Experimentation/Global Energy and Water Cycle Experiment Atmospheric System Study (WGNE and MJO-Task Force/GASS) global model comparison project. For this, intraseasonal moisture budget equation is analyzed and a simple, efficient physical quantity is developed. The result shows that MJO skill is most sensitive to vertically integrated intraseasonal zonal wind convergence (ZC). In particular, a specific threshold value of the strength of the ZC can be used as distinguishing between good and poor models. An additional finding is that good models exhibit the correct simultaneous convection and large-scale circulation phase relationship. In poor models, however, the peak circulation response appears 3 days after peak rainfall, suggesting unfavorable coupling between convection and circulation. For an improving simulation of the MJO in climate models, we propose that this delay of circulation in response to convection needs to be corrected in the cumulus parameterization scheme.

Keywords Madden–Julian oscillation · YOTC/MJO-TF · Climate models · Zonal wind convergence · Coupling between convection and circulation · Cumulus parameterization scheme

✉ Kyong-Hwan Seo
khseo@pusan.ac.kr

[1] Department of Atmospheric Sciences, Pusan National University, Busan 609-735, South Korea

1 Introduction

The Madden–Julian oscillation (MJO) is the most dominant mode of intraseasonal variability in the tropics (Madden and Julian 1994; Zhang 2005). The MJO strongly affects the weather and climate in high-latitudes and polar regions in addition to those over the tropics and mid-latitudes through meridionally propagating Rossby waves and equatorial Rossby and Kelvin waves, respectively (Maloney and Hartmann 2000; Jones et al. 2004; Hendon et al. 2007; Seo and Wang 2010; Wheeler and McBride 2011; Seo and Son 2012; Yoo et al. 2012; Seo et al. 2016). Because of its global impact, proper simulation of the MJO is imperative for improving the prediction performance of general circulation atmospheric models (GCMs) and atmosphere–ocean coupled models. For example, in the National Centers for Environmental Prediction Climate Forecast System (NCEP CFS), a coupled model that realistically simulated MJO, the simulated upper-level circulation pattern correlated with observation at a level of 0.85–0.90. The results demonstrate that the realistically simulated MJO improves the simulation of global circulation pattern through Rossby wave propagation (Seo and Wang 2010). However, state-of-the-art GCMs or coupled models still have difficulty in producing accurate MJO convection and circulation anomalies (Lin et al. 2006; Seo et al. 2007; Kim et al. 2009; Seo and Wang 2010; Hung et al. 2013; Jiang et al. 2015). Only one model participating in Phase 5 of the Coupled Model Intercomparison Project (CMIP5) of the Intergovernmental Panel on Climate Change (IPCC) simulation project has simulated a reasonable eastward propagation of the MJO (Hung et al. 2013).

To resolve this problem, the Working Group on Numerical Experimentation (WGNE), and the MJO Task Force (MJO-TF), under the auspices of the Year

Published online: 19 March 2017

of Tropical Convection (YOTC) (Moncrieff et al. 2012; Waliser et al. 2012) and the GEWEX Atmospheric System Study (GASS), developed modeling experiments and compared MJO simulation skill. By using 20-year climate simulation data from 27 different GCMs, Jiang et al. (2015) demonstrated that models having more realistic MJO effectively reproduced the vertically westward tilted structure in zonal wind, temperature, vertical pressure velocity, diabatic heating, and specific humidity relative to intraseasonal convection. The tilted structure has resulted from the boundary layer moisture convergence to the east of MJO convection, preconditioning the atmosphere for subsequent shallow and deep convection. An MJO skill score, measured by the ratio of the eastward propagating intraseasonal signal to the westward counterpart, was shown to correlate with the difference in low-level relative humidity between heavy and light rainfall events. The seasonal mean gross moist stability also exhibited a significant relationship with the MJO skill score. However, their correlation is about 0.45, explaining only 20% of the total variation. So, a specific physical process sensitive to the MJO simulation performance still has not been fully addressed. As stated in DeMott et al. (2015), it is extremely difficult to detect a single feature that links highly or poorly performing models in simulating MJO since the related processes are complex.

The present study aims to identify a single essential physical factor that can distinguish between highly performing and poorly performing models by using the aforementioned 20-year simulation data. For this purpose, a moisture budget equation is used and a key process sensitive to simulating realistic MJO is examined to provide insight into MJO simulation.

2 Datasets and methods

Observational and reanalysis datasets used for the period 1998–2012 include winds and specific humidity from the European Center for Medium range Weather Forecasts Re-analysis-Interim (ERA-Interim) (Dee et al. 2011) and rainfall data from the ERA-Interim, the Tropical Rainfall Measuring Mission (TRMM) 3B42 version 7 (Huffman et al. 2007), and the Global Precipitation Climatology Project (GPCP) version 1.2 (Huffman et al. 2001). Although the rainfall data of the TRMM and GPCP are of better quality than those of ERA-Interim, the latter was used in this study for constructing a dynamically consistent field with other variables, as was done in Kim et al. (2014).

The model datasets are 20-year data from 26 different climate simulations participating in the WGNE (MJO-TF)/GASS MJO global model comparison project. Different from that reported by Jiang et al. (2015), the MetUM-GA3 model is excluded from the present study owing to an excessive amount of missing data. Detailed information about the 26 climate simulations can be found in Jiang et al. (2015). All datasets provide daily data with a 2.5°×2.5° longitude–latitude grid at 20 vertical pressure levels from 975 to 100 hPa. The analyses are performed during the boreal winter season from November to the following April. Data at 1000 hPa are excluded from the calculation because the lower boundary in some models is lower than that value. The use of the extrapolated data to 1000 hPa does not change any of the major features presented.

We begin by analyzing the vertically integrated moisture budget equation, in which each term is presented as an equal unit of W m^{-2} by multiplying the latent heat of condensation (L),

$$\left[\frac{\partial(Lq)}{\partial t}\right] = -\left[\vec{V}_H \cdot \nabla(Lq)\right] - \left[(Lq)\nabla \cdot \vec{V}_H\right] - \mathrm{LP} + \mathrm{LH} \quad (1)$$

where q is specific humidity, $\vec{V}_H$ is the horizontal wind vector, ∇ is the horizontal gradient operator, LH is surface latent heat flux, and P is precipitation at the surface. The square brackets indicate a mass-weighted vertical integral from 975 to 500 hPa. Due to a scarcity of water vapor in the upper troposphere, the results using integration from 975 to 100 hPa are almost the same (not shown). The left term is the vertically integrated moisture tendency (MT). The first and second terms with negative signs on the right-hand side are the vertically integrated horizontal moisture advection (MA) and horizontal moisture convergence (MC).

We tried to apply the above equations to examine a significant physical factor using total anomaly data (i.e., with no bandpass filtering) (not shown); however, it was hard to find any significant sensitivity in differentiating models with good and bad performance due to existence of strong low-frequency variability (>100 day) in this total anomaly. As an ad-hoc approach, we used the intraseasonally filtered anomalies to utilize the above equation in this study. The anomalies for each variable are derived by removing the annual cycle, which is composed of the time mean and first three annual harmonics, and the intraseasonal variation is then extracted by using a 20–100 day bandpass filter. Again, continued effort needs to find a factor using unfiltered data in the future.

To examine the sensitivity of the MJO simulation skill to physical factors, we divide the models into highly performing and poorly performing models based on three previously developed metrics (Table 1). The first is the ratio of eastward to westward power (E/W ratio) (Kim et al. 2009; Jiang et al. 2015), which is the most widely used criterion as an MJO skill measure. This ratio is estimated by calculating the strength of eastward and westward power signals of zonal wavenumbers from 1 to 3 and periods between 30 and 60 days from a space–time spectrum for

Table 1 Summary of model ranking for various Madden–Julian oscillation (MJO) simulation skill measures including the ratio of eastward to westward power (E/W ratio), pattern correlation of regressed rainfall and maximum lead–lag correlation between the first and second principal components (PC1 and PC2) of the empirical orthogonal function (EOF) of outgoing longwave radiation (OLR), denoted as R_{max}

No.	Model name	E/W ratio	Pattern corr. of regressed rainfall	R_{max}
3	ACCESS1	16	15	11
4	BCC-AGCM2.1	11	21	8
5	*CAM5*	19	18	23
6	*CAM5-ZM*	21	14	22
7	*CanCM4**	23	22	20
8	*CFS2*	22	26	21
9	CNRM-ACM	9	11	18
10	CNRM-AM	14	13	14
11	**CNRM-CM***	2	6	2
12	*CWB-GFS*	20	23	25
13	ECEarth3	15	10	10
14	EC-GEM	18	19	13
15	**ECHAM5-SIT***	6	4	3
16	ECHAM6*	10	12	16
17	FGOALS-s2	17	8	12
18	*GEOS5*	25	17	24
19	**GISS-E2**	3	1	4
20	ISUGCM	13	20	17
21	*MIROC5*	26	24	26
22	**MRI-AGCM3**	8	7	15
23	*NavGEM1*	24	25	19
24	**PNU-CFS***	4	9	7
25	**SPCAM3**	7	3	5
26	**SPCCSM3***	5	2	6
27	**TAMU-CAM4**	1	5	1
28	UCSD-CAM3	12	16	9

Coupled models are denoted by an asterisk; otherwise, the model is an atmospheric general circulation model (GCM). Good (poor) models are expressed in bold (italics). Good and poor models were chosen when at least two criteria among the three were met as the top and bottom 30% ranking

rainfall of the global tropics (i.e., 0–360°E, 15°S–15°N). The second metric is the pattern correlation of regressed rainfall used in Jiang et al. (2015). For this, rainfall anomalies averaged over 10°S–10°N are regressed onto time series of 20–100-day bandpass filtered rainfall averaged over the eastern Indian Ocean (80°–90°E, 5°S–5°N). The time–longitude field of the regressed rainfall anomaly is then prepared for lag days −20 to 20. This pattern is compared with ERA-Interim to obtain the pattern correlation. The same procedure is applied to the western Pacific base region (135°–145°E, 5°S–5°N), and the final skill score is the average value of the two pattern correlations. The last metric is the maximum lead–lag correlation between the first and second principal components (PC1 and PC2) of the empirical orthogonal function (EOF) of outgoing longwave radiation (OLR), denoted as R_{max} (Sperber and Kim 2012). Inclusion of other measures of MJO skill such as eastward power (Kim et al. 2014) and the ratio of squared eastward power to westward power (Sperber and Kim 2012) does not change the overall results. On the basis of these three criteria, the models constituting the top and bottom 30% are selected as good and poor models, respectively (Table 1). The eight good models include CNRM-CM, ECHAM5-SIT, GISS-E2, MRI-AGCM3, PNU-CFS, SPCAM3, SPCCSM3, and TAMU-CAM4; poor models are CAM5, CAM5-ZM, CanCM4, CFS2, CWB-GFS, GEOS5, MIROC5, and NavGEM1. The models selected as good are the same as those reported by Jiang et al. (2015), although the poor models differ slightly.

In Tables 1 and 2 and Figs. 1–5, the observation or reanalysis rainfall data of TRMM, GPCP, and ERA-Interim are numbered 0, 1, and 2, respectively; those of climate models are numbered 3–28.

3 Results

We first identify the MJO life cycle through lead–lag regression of the vertically integrated moisture budget terms calculated over the Indian Ocean (IO) (65°–105°E, 10°S–10°N), as shown in Fig. 1. The used index in this study is the normalized time series of 20–100 day bandpass-filtered ERA-interim rainfall anomalies averaged over the IO (65°–105°E, 10°S–10°N). All variables exhibit pronounced cyclic behavior, implying moistening and drying of the atmosphere. The MA becomes positive about 3 weeks prior to the occurrence of maximum rainfall (equivalently, to the east of maximum rainfall in space) and peaks at day −10, which contributes to similar phase evolution of the MT. At approximately days −20 to −7, an easterly anomaly at the surface acts to reduce the total wind speed so that the LH is negative, whereas under and west of the peak MJO convection (lag days −6 to 10), westerly anomaly tends to increase the total wind speed, leading to the positive LH (not shown). The MC and rainfall show an approximately in-phase relationship and lag the MA and MT terms by a quarter of a cycle. All of these features are consistent with previous findings (e.g., Benedict and Randall 2011; Seo et al. 2007; DeMott et al. 2015). The temporal patterns (or equivalently spatial patterns) from the moisture budget are similar to those from the moist static energy or the moist entropy budget equation (Maloney 2009; Kiranmayi and Maloney 2011; Benedict et al. 2014; DeMott et al. 2014).

Table 2 List of YOTC/MJO-TF climate models with convection and closure schemes. For the references in the table, refer to Jiang et al. (2015)

No.	Model name	Convection scheme/modification	Convective closure
3	ACCESS1	Gregory and Rowntree (1990)	CAPE
4	BCC-AGCM2.1	Zhang and McFarlane (1995)/Zhang and Mu (2005)	CAPE
5	*CAM5*	Zhang and McFarlane (1995)/Richter and Rasch (2008)	CAPE
6	*CAM5-ZM*	Zhang and McFarlane (1995)/Neale et al. (2008)	CAPE
7	*CanCM4**	Zhang and McFarlane (1995)	CAPE
8	*CFS2*	Hong and Pan (1998)	Entraining CAPE
9	CNRM-ACM	Bougeault (1985)	Kuo type
10	CNRM-AM	Bougeault (1985)	Kuo type
11	**CNRM-CM***	Bougeault (1985)	Kuo type
12	*CWB-GFS*	Pan and Wu (1995)	Entraining CAPE
13	ECEarth3	Bechtold et al. (2004)	CAPE
14	EC-GEM	Fritsch and Chappell (1980)	CAPE
15	**ECHAM5-SIT***	Tiedtke (1989)/Nordeng (1994)	CAPE
16	ECHAM6*	Tiedtke (1989)/Nordeng (1994)	CAPE
17	FGOALS-s2	Tiedtke (1989)/Nordeng (1994)	CAPE
18	*GEOS5*	Moorthi and Suarez (1992)	Entraining CAPE
19	**GISS-E2**	Del Genio and Yao (1993)	Entraining CAPE
20	ISUGCM	Zhang and McFarlane (1995)/Zhang and Wu (2003)	CAPE
21	*MIROC5*	Chikira and Sugiyama (2010)	CAPE
22	**MRI-AGCM3**	Yukimoto et al. (2011)	Entraining CAPE
23	*NavGEM1*	Hong and Pan (1998)	Entraining CAPE
24	**PNU-CFS***	Moorthi and Suarez (1992)	Entraining CAPE
25	**SPCAM3**	Khairoutdinov and Randall (2003)	Non-equilibrium
26	**SPCCSM3***	Khairoutdinov and Randall (2001, 2003)	Non-equilibrium
27	**TAMU-CAM4**	Zhang and McFarlane (1995)/Richter and Rasch (2008)	Entraining CAPE
28	UCSD-CAM3	Zhang and McFarlane (1995)	CAPE

To simplify the sensitivity investigation of a model's MJO simulation performance to the aforementioned physical processes, we select the time interval of a full cycle over which the rainfall anomalies evolve (Fig. 1) with lag days −16 to 16. Then, to avoid cancellation of the positive and negative values the absolute value of the regressed anomalies is taken for each term. Next, the positive value is averaged over this time span to represent the strength of each term. This calculation is possible because the lead–lag relationships of the vertically integrated moisture budget terms with respect to the intraseasonal rainfall anomaly for each model are similar to those in the ERA-Interim data (Figs. 1, 2). Use of TRMM or GPCP as the rainfall index produces similar results to those shown in Fig. 1. Therefore, the detailed phase difference against the intraseasonal rainfall anomaly does not need to be considered. This enables the statistics to be less sensitive to any specific phase, which makes the calculations are more feasible. The result is not sensitive to the addition or exclusion of a few days in the MJO cycle.

On this basis, a scatter diagram between the E/W ratio (ordinate) and the strength of each physical term (abscissa) over the IO for the observation, reanalysis and GCM simulations is plotted in Fig. 3. The correlation coefficients for the MA and MC with the E/W ratio are 0.79 and 0.88 (MT for 0.71, LH for 0.37; not shown). Note that although the rainfall is also highly correlated with the E/W ratio, we do not consider this term since rainfall is end product of complex processes in model integrations and we intend to find a specific process demonstrating the sensitivity other than this rainfall. The MC has higher correlation with the E/W ratio than the other four terms during the MJO cycle. It appears that the MC term is capable of classifying highly and poorly performing models in simulating the MJO (Fig. 3b). However, a careful examination reveals that although the observation and reanalysis (green colors in Fig. 3) have a large E/W ratio, the strength of the MC (abscissa) overlaps the middle group models 3, 9, 16, and 28 and one bad model, model 12. Then, we examine the relative contribution to the intraseasonal MC term by decomposing into three different time scales:

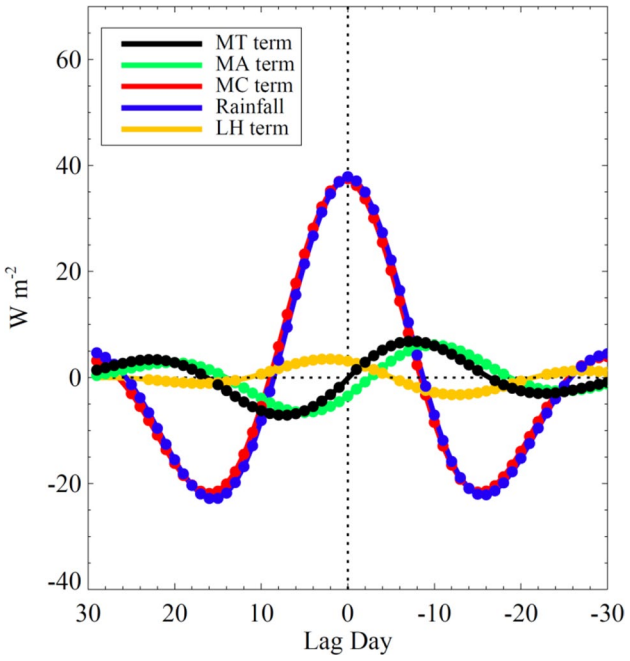

Fig. 1 Time evolution of vertically integrated (975–500 hPa) intraseasonal moisture budget terms regressed onto time series of 20–100 day filtered rainfall anomalies over the central Indian Ocean (65°–105°E, 10°S–10°N) based on ERA-Interim. Moisture tendency (MT) is denoted by the *black line*, moisture advection (MA) is in *green*, moisture convergence (MC) is in *red*, rainfall is in *blue*, and surface latent heat flux (LH) is in *yellow*. Solid circles in each color denote statistically significant points at the 90% level based on Student's *t* test. All units are in W m^{-2}. The lag days in the abscissa were reversed to match the zonal structure

$$-\left\{\left[Lq\nabla\cdot\vec{\mathrm{V}}_{\mathrm{H}}\right]\right\}\approx-\left\{\left[L\bar{q}\nabla\cdot\left\{\vec{\mathrm{V}}_{\mathrm{H}}\right\}\right]\right\}-\left\{\left[\left\{Lq\right\}\nabla\cdot\overline{\vec{\mathrm{V}}_{\mathrm{H}}}\right]\right\}-\left\{\left[\left\{Lq'\nabla\cdot\vec{\mathrm{V}}_{\mathrm{H}}{}'\right\}\right]\right\} \quad (2)$$

where the overbar denotes the boreal winter time mean, the prime represents the total anomaly, and the brackets indicate the 20–100 day filtered anomaly. On the right-hand side of Eq. (2), the first term is the convergence of mean moisture by the MJO horizontal wind, which is a dominant term. This term is strongly correlated with E/W ratio (0.86, not shown). This is further divided into convergence by zonal and meridional wind components, $-\left[L\bar{q}\,\partial\{u\}/\partial x\right]$ and $-\left[L\bar{q}\,\partial\{v\}/\partial y\right]$, respectively. The correlation of the convergence by the MJO zonal wind with the E/W ratio is as high as 0.83 (Fig. 3c), whereas that by the MJO meridional wind is nearly zero (not shown).

A further decomposition of this MC (i.e., $-\left[L\bar{q}\,\partial\{u\}/\partial x\right]$) shows that the ZC ($-\left[\partial\{u\}/\partial x\right]$) is dominant with a correlation of 0.85 (Fig. 3d), whereas the E/W ratio is not sensitive to time mean moisture ($\left[\bar{q}\right]$, Fig. 3e). It should be noted that the ZC term (Fig. 3d) shows a higher correlation with the E/W ratio and is able to categorize the good and poor models according to a threshold value of ZC strength, such as 8 kg m^{-2} s^{-1}. Meanwhile, the zonal wind itself (Fig. 3f) does not clearly discriminate good or poor models, although it is strongly correlated with the E/W ratio. To summarize, the magnitude of the ZC (i.e., intraseasonal ZC) during the MJO cycle is the most important factor in distinguishing highly or poorly performing models for the simulation of the MJO. Note that if the outlier models (TAMU-CAM4) is excluded in the linear fit in Fig. 3, the correlation coefficients are only slightly reduced so the major results are not changed.

Figure 4 illustrates the life cycle of MJO convection and circulation anomalies for the TRMM/ERA-Interim (hereafter, simply referred to as the reanalysis) and good and poor models to investigate the spatial relationship between convection and circulation during the MJO cycle. For this calculation, rainfall, horizontal wind, and zonal wind convergence at 70 0 hPa are regressed onto the same normalized rainfall index as that used in Fig. 1. The evolution is divided into four stages including phases of suppression and initiation (lag days −20 to −12), development (days −12 to −4), peak (days −4 to 5), and decay (days 5 to 14). These results are not sensitive to the specific choice of vertical level or lag days. During the suppression and initiation phase in the reanalysis, the suppressed convection is located over the eastern IO, and the easterly anomalies appear to the west of the suppressed convection as a Rossby wave response. The easterly anomaly tends to decrease toward the western IO, particularly along 5°S, leading to zonal wind convergence and the initiation of new MJO convection in the western IO. This result is exactly consistent with the downstream forcing mechanism proposed as an MJO initiation mechanism by Zhao et al. (2013). At this phase, the good model composite shown in Fig. 4b exhibits similar dipole convection and zonal wind patterns as those in the reanalysis, whereas the poor model composite in Fig. 4c show very weak convective and circulation signals.

During the development and peak phases, the observed zonal wind convergence (shading) strengthens owing to more enhanced convection (contours) over the IO. This feature is also evident in the good model composite; even the suppressed convection over the western Pacific is well simulated. In contrast, the poor models show significantly weaker convection and zonal wind convergence with the convective cell and related convergence region (red shading) moving toward the west. The suppressed convection in the western Pacific is not well seen in this poor model composite. The decay phase is characterized by the appearance of suppressed convection and the resultant zonal wind divergence over the IO. The good model results are similar to the reanalysis, whereas in the poor models, the

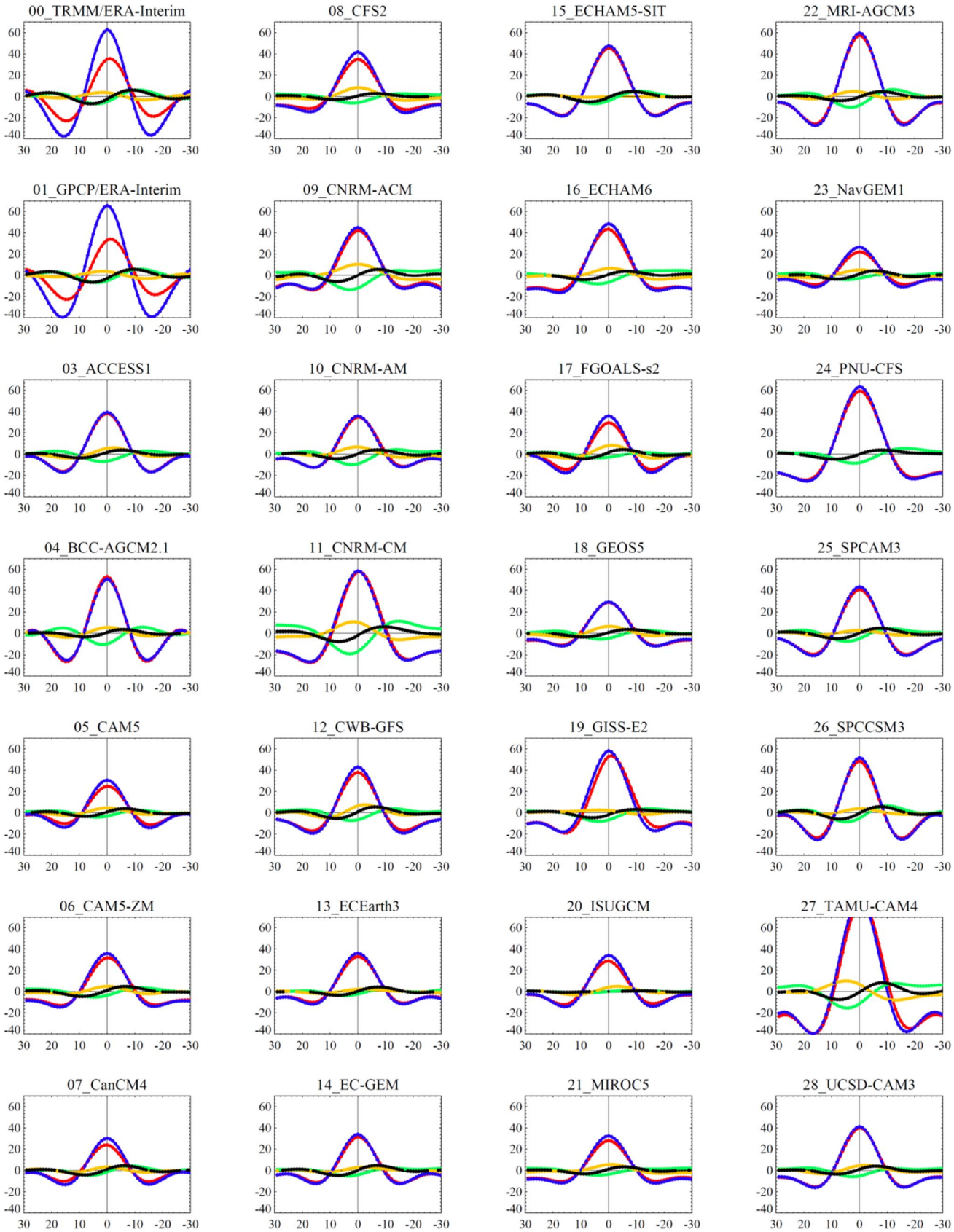

Fig. 2 Same as in Fig. 1, but for TRMM, GPCP and 26 GCMs

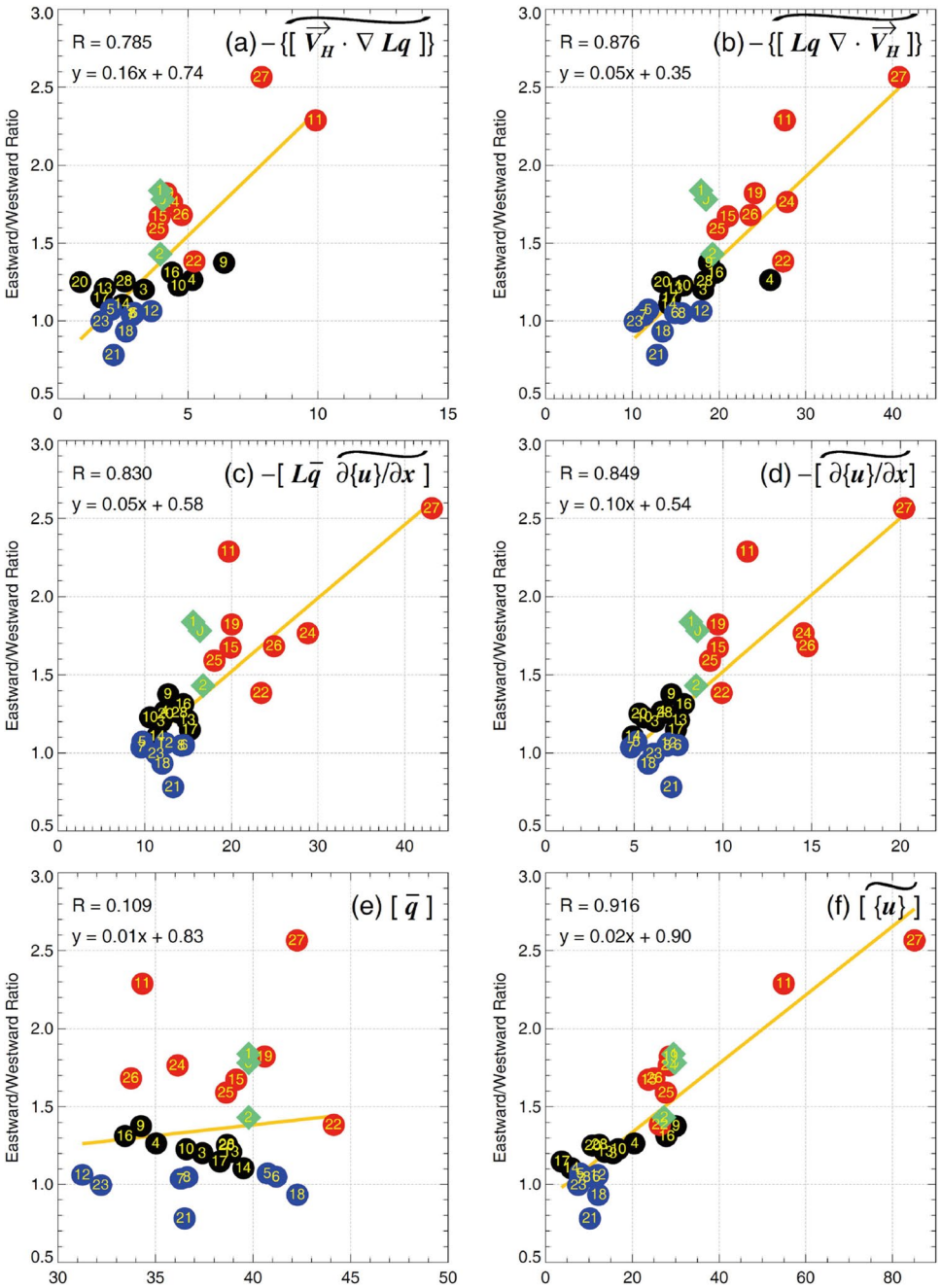

Fig. 3 Scatter diagram between the E/W ratio and **a** MA, **b** MC, **c** moisture convergence by MJO zonal wind, **d** zonal wind convergence (ZC), **e** time-mean moisture, and **f** MJO zonal wind. All quantities are averages over a full cycle of rainfall evolution over the Indian Ocean. *Filled green diamonds* represent observation and reanalysis data, and filled circles denote each model simulation. *Red* (*blue*) *filled circle* denote good (poor) models, and tildes represent one cycle of rainfall evolution. The linear correlation coefficient (R) is presented in the plot. For **a, b**, and **c** units are in W m^{-2}; those in **d** are in 10^{-4} kg m^{-2} s^{-1}; those in **e** are kg m^{-2}; and those in **f** are in 10^2 kg m^{-1} s^{-1}

rainfall anomaly disappears, and the zonal wind convergence moves to the west in the IO.

To better describe the evolution difference between the good and poor models, a life cycle in a phase diagram composed of the regressed rainfall and ZC over the IO (65°–105°E, 10°S–10°N) is presented in Fig. 5 for lag days from −16 to 16. During the development and peak (decay) phases, a sharp increase (decrease) in the rainfall and vertically integrated (975–500 hPa) ZC is exhibited in both reanalysis and the good models, whereas the poor models show significantly slower increase (decrease) at an initial (decaying) phase. The reanalysis and good models exhibit an enormously compact cycle along the diagonal direction with the evolution trajectory passing the origin nearby, suggesting that the evolution pattern is consistent with a discharge–recharge mechanism (Benedict and Randall 2007; Thayer-Calder and Randall 2009) and a quasi-linear property between the enhanced and suppressed MJO stages. In contrast, the poor models show a rather elliptical evolution, with significantly smaller magnitudes of rainfall and ZC than those in the good models.

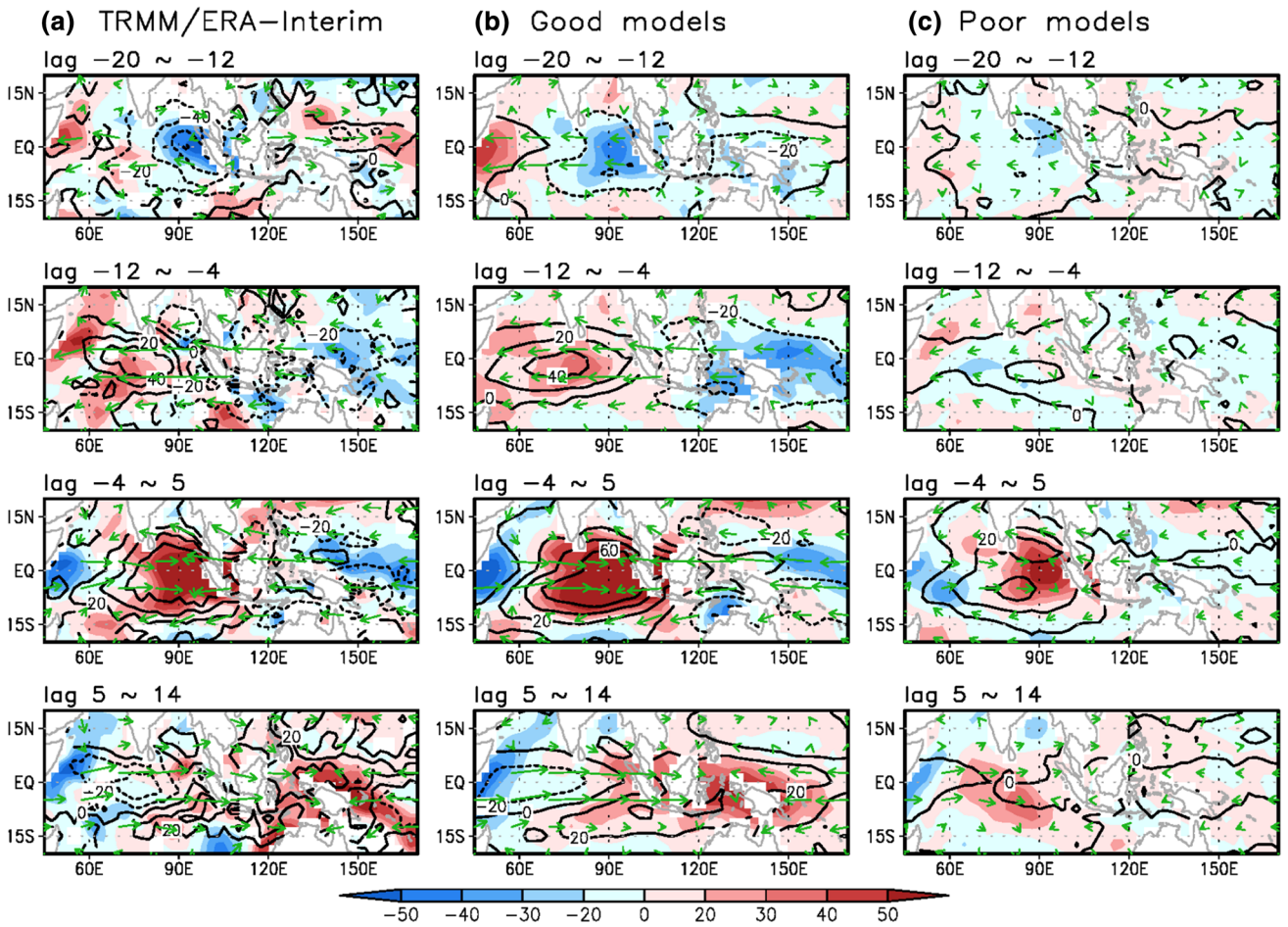

Fig. 4 Longitude–latitude plot of intraseasonal zonal wind convergence (shaded, intervals of 1×10^{-8} s^{-1}), wind (green vector, intervals of 3 m s^{-1} in TRMM/ERA-Interim (hereafter, simply referred to as reanalysis) and 4 m s^{-1} in models), and rainfall (*black* contours, intervals of 20 W m^{-2}) at 700 hPa regressed onto time series of the 20–100-day bandpass filtered rainfall for **a** the reanalysis, **b** the good models, and **c** the poor models. All variables are statistically significant above the 90% level

A more important feature shown in Fig. 5 is that the maximum ZC (a square) occurs simultaneously with the peak rainfall (i.e., lag day 0, a cross) in the good models and in the reanalysis. In the poor models, however, the maximum ZC appears 3 days after the peak rainfall; thus, the developing convection is not immediately supported by ZC, which limits further development of convection and leads to subsequent reduction in the circulation response. The convection–circulation phase difference hindered the correct coupling between them and suggested that the quasi-stationary (or westward propagating, see Fig. 4) convective and circulation signals in the poor models (Guo et al. 2015; Jiang et al. 2015). An inspection of individual poor models reveals that the maximum ZC lags behind the peak rainfall by 2–4 days; 4 of the 8 poor models have a 4-day lag bias. By contrast, eight good models exhibit a minus 1 to 1-day lags (not shown).

This inconsistency between convection and large-scale circulation comes from multiple causes including an inappropriate treatment of various components inside deep convective parameterization scheme and an incomplete representation of small-scale contribution to large-scale variables or their interactions. It may include the following limitation: in nature, the cumulus convection process such as transition from shallow to deep convection is gradual but model simulates this differently with the observation.

As shown in Table 2, no particular scheme is given a credit for better simulating the MJO variability: the good models use Kuo-type moisture convergence scheme or mass-flux scheme such as Relaxed Arakawa–Schubert and Zhang and McFarlane schemes and the poor models employ the similar schemes. Therefore, it is almost impossible to pinpoint a specific element as a major culprit. However, we speculate that some degree of improvement can be achieved by performing a proper adjustment or change

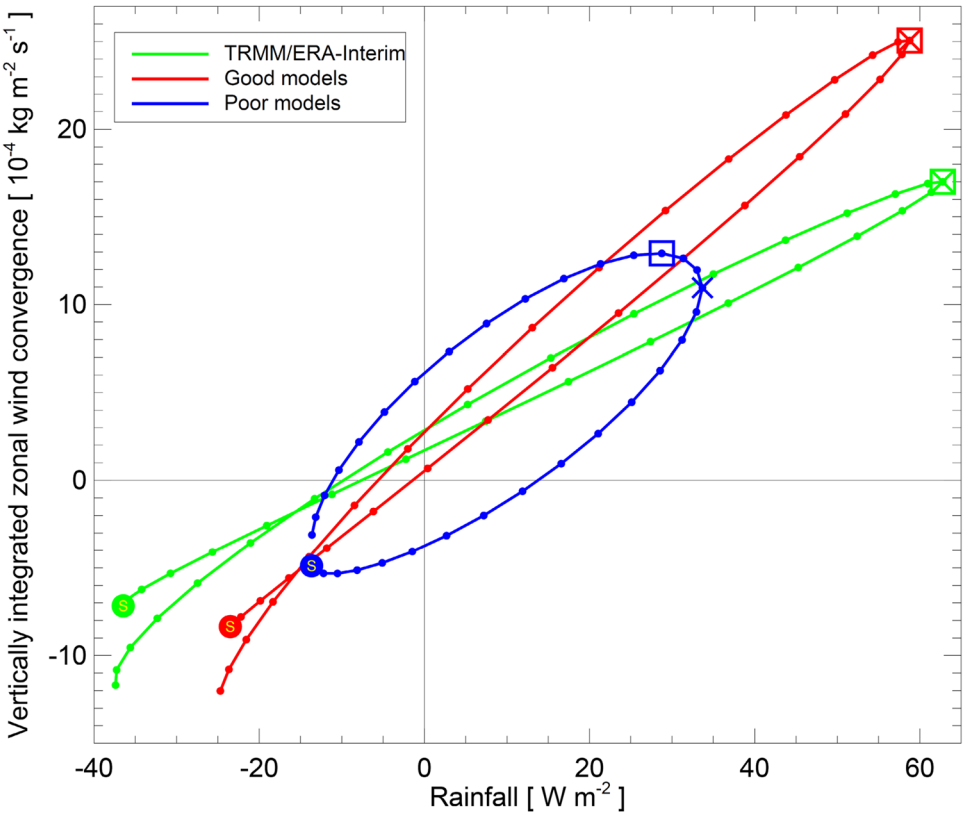

Fig. 5 Relationship between rainfall and ZC regressed onto the time series of 20–100-day filtered rainfall anomalies over the Indian Ocean (IO) (65°–105°E, 10°S–10°N) for one cycle of rainfall evolution for the reanalysis (*green*), good models (*red*), and poor models (*blue*). All fields are intraseasonal anomalies averaged over the same IO box. Each filled small circle represents 1 day. "S" indicates day −16, "×" denotes a maximum rainfall day, and the large *open square* denotes the maximum ZC day. The unit of rainfall is W m^{-2}; that of ZC is 10^{-4} kg m^{-2} s^{-1}

of "a closure" in the deep convection parameterization scheme. For example, a quasi-equilibrium hypothesis for the closure of mass flux scheme may not always work on the intraseasonal time scale. As one of metrics for evaluating GCM performance, we suggest that the in-phase relationship between the deep convection and large-scale convergence on this subseasonal time scale needs to be checked. Elucidation of an exact reason for this deficiency in some models is left for future study.

4 Summary and discussion

A key physical factor in regulating the performance of MJO is examined by using 26 climate model simulations. For this study, an intraseasonal moisture budget equation is considered, and a simple, efficient physical quantity is developed to assess the sensitivity of the MJO performance. Each term in this equation is first regressed onto the time series of rainfall over the central tropical IO, and the absolute value of the regressed anomalies over a full cycle of rainfall evolution is then averaged to represent the strength of each term. Most of the model simulation data analyzed in this study exhibit the similar phase relationships among the budget terms as shown in the reanalysis data (see Figs. 1, 2), leading to feasibility of expressing one or two metrics to synthesize the evolution feature.

The results show that the intraseasonal ZC, vertically integrated from 925 to 500 hPa, is able to clearly distinguish highly performing models and poorly performing models. The ZC term exhibits a higher correlation with the E/W ratio and is able to categorize the good and poor models according to a threshold value of ZC strength at 8 kg m^{-2} s^{-1}. Composite analysis demonstrates that the pattern and magnitude of convection and circulation anomalies in the good models are similar to those in the reanalysis with a sharp increase (decrease) in the rainfall and ZC during the development and peak (decay) phases. This result is consistent with the discharge-recharge mechanism. However, the poor models show stationary or westward propagating anomalies and a zonally narrow pattern with significantly weaker amplitude than that in the good models at all stages.

An important finding in this study is that an average 3-day delay appears in the circulation field in response to convective forcing in the poor models. However, the good models exhibit an accurate, simultaneous convection and large-scale circulation phase relationship such that the robust coupling between convection and circulation enables the MJO to sustain against dissipation. The inconsistency between the convection and circulation in the poor models can be attributed to the unrealistic treatment in the deep convection parameterization scheme.

The high correlation (Fig. 3d) on its own is a little bit hard to interpret presumably since the calculation is done for one cycle of MJO precipitation, so it does not seem to explicitly provide differences in related physical processes. However, if the daily evolution within this cycle as shown in Fig. 5 is considered, a more clear difference in the physical states emerges between good and poor models. So, this ultimately gives a meaningful convection–circulation state that each model produces.

Recent studies have demonstrated that although the environmental relative humidity difference may be hard to distinguish the MJO performance in the model, the environmental relative humidity is sensitive components for simulating MJO (Kim et al. 2014; Maloney et al. 2014; Jiang et al. 2015). The low-level (850–700 hPa) relative humidity (RH) difference is defined between upper 10% (strong) and lower 20% (weak) of rainfall events over the Indian Ocean [65°–105°E, 10°S–10°N]. The low-level RH difference has a correlation of 0.34 with the E/W ratio (not shown). Most good models and two poor models (model numbers 5 and 6) simulated a low-level RH difference between 30 and 40%. It suggests that the model performance is not sensitive to the RH difference factor. These results are consistent with the previous study of Jiang et al. 2015 (in their Fig. 10b).

The current study provides insight into the primary physical elements for improved MJO simulation in climate models. Although it remains extremely difficult to pinpoint a specific component in cumulus parameterization, a closure scheme is suggested to be thoroughly examined and improved.

Acknowledgements This work was supported by the National Research Foundation of Korea (NRF) grants funded by the Korea government (MSIP) (No. NRF-2014R1A2A1A11051818 & No. NRF-2015R1A2A2A01006663). We would like to acknowledge the support from the Korea Institute of Science and Technology Information (KISTI). We are very grateful to the two anonymous reviewers for their helpful and constructive comments, which contributed to improving this paper.

References

Bechtold P, Chaboureau JP, Beljaars ACM, Betts AK, Köhler M, Miller M, Redelsperger JL (2004) The simulation of the diurnal cycle of convective precipitation over land in global models. Q J R Meteorol Soc 130:3119–3137

Benedict JJ, Randall DA (2007) Observed characteristics of the MJO relative to maximum rainfall. J Atmos Sci 64:2332–2354

Benedict JJ, Randall DA (2011) Impacts of idealized air-sea coupling on Madden-Julian oscillation structure in the superparameterized CAM. J Atmos Sci 68:1990–2008

Benedict JJ, Maloney ED, Sobel AH, Frierson DMW (2014) Gross moist stability and MJO simulation skill in three full-physics GCMs. J Atmos Sci 71:3327–3349

Bougeault P (1985) A simple parameterization of the large-scale effects of cumulus convection. Mon Weather Rev 113:2108–2121

Chikira M, Sugiyama M (2010) A cumulus parameterization with state-dependent entrainment rate. Part I: description and sensitivity to temperature and humidity profiles. J Atmos Sci 67:2171–2193

Dee DP et al (2011) The ERA-Interim reanalysis: configuration and performance of the data assimilation system. Q J R Meteorol Soc 137:553–597

Del Genio AD, Yao MS (1993) Efficient cumulus parameterization for long-term climate studies: the GISS scheme. In: Emanuel K, Raymond D (eds) The representation of cumulus convection in numerical models, Meteorological Monographs, vol 24. American Meteorological Society, Boston, pp 181–184

DeMott CA, Stan C, Randall DA, Branson MD (2014) Intraseasonal variability in coupled GCMs: the roles of ocean feedbacks and model physics. J Clim 27:4970–4995. doi:10.1175/jcli-d-13-00760.1

DeMott CA, Klingaman NP, Woolnough SJ (2015) Atmosphere-ocean coupled processes in the Madden-Julian oscillation. Rev Geophys 53:1099–1154. doi:10.1002/2014RG000478

Fritsch JM, Chappell CF (1980) Numerical prediction of convectively driven mesoscale pressure systems. Part I: Convective parameterization. J Atmos Sci 37:1722–1733

Gregory D, Rowntree PR (1990) A mass flux convection scheme with representation of cloud ensemble characteristics and stability-dependent closure. Mon Weather Rev 118:1483–1506

Guo Y, Waliser DE, Jiang X (2015) A systematic relationship between the representations of convectively coupled equatorial wave activity and the Madden-Julian oscillation in climate model simulations. J Clim 28:1881–1904

Hendon HH, Wheeler MC, Zhang C (2007) Seasonal dependence of the MJO-ENSO relationship. J Clim 20:531–543

Hong S-Y, Pan H-L (1998) Convective trigger function for a mass-flux cumulus parameterization scheme. Mon Weather Rev 126:2599–2620

Huffman GJ, Adler RF, Morrissey MM, Bolvin DT, Curtis S, Joyce R, McGavock B, Susskind J (2001) Global precipitation at one-degree daily resolution from multisatellite observations. J Hydrometeor 2:36–50

Huffman GJ, Adler RF, Bolvin DT, Gu G, Nelkin EJ, Bowman KP, Hong Y, Stocker EF, Wolff DB (2007) The TRMM multisatellite precipitation analysis (TMPA): quasi-global, multiyear, combined-sensor precipitation estimates at fine scales. J Hydrometeor 8:38–55

Hung M-P, Lin J-L, Wang W, Kim D, Shinoda T, Weaver SJ (2013) MJO and convectively coupled equatorial waves simulated by CMIP5 climate models. J Clim 26:6185–6214

Jiang X et al (2015) Vertical structure and physical processes of the Madden-Julian oscillation: exploring key model physics in climate simulations. J Geophys Res Atmos 120:4718–4748. doi:10.1002/2014JD022375

Jones C, Waliser DE, Lau KM, Stern W (2004) Global occurrences of extreme precipitation and the Madden-Julian oscillation: observations and predictability. J Clim 17:4575–4589

Khairoutdinov MF, Randall DA (2001) A cloud resolving model as a cloud parameterization in the NCAR Community Climate System Model: preliminary results. Geophys Res Lett 28:3617–3620

Khairoutdinov MF, Randall DA (2003) Cloud-resolving modeling of ARM Summer 1997 IOP: model formulation, results, uncertainties and sensitivities. J Atmos Sci 60:607–625

Kim D et al (2009) Application of MJO simulation diagnostics to climate models. J Clim 22:6413–6436

Kim D et al (2014) Process-oriented MJO simulation diagnostic: moisture sensitivity of simulated convection. J Clim 27:5379–5395

Kiranmayi L, Maloney ED (2011) Intraseasonal moist static energy budget in reanalysis data. J Geophys Res Atmos 116:D21117. doi:10.1029/2011JD016031

Lin J-L et al (2006) Tropical intraseasonal variability in 14 IPCC AR4 climate models Part I: convective signals. J Clim 19:2665–2690

Madden RA, Julian PR (1994) Observations of the 40-50-day tropical oscillation: a review. Mon Weather Rev 122:814–837

Maloney ED (2009) The moist static energy budget of a composite tropical intraseasonal oscillation in a climate model. J Clim 22:711–729

Maloney ED, Hartmann DL (2000) Modulation of eastern North Pacific hurricanes by the Madden-Julian oscillation. J Clim 13:1451–1460

Maloney ED, Jiang X, Xie SP, Benedict JJ (2014) Process-oriented diagnosis of East Pacific warm pool intraseasonal variability. J Clim 27:6305–6324

Moncrieff MW, Waliser DE, Miller MJ, Shapiro MA, Asrar GR, Caughey J (2012) Multiscale convective organization and the YOTC virtual global field campaign. Bull Am Meteorol Soc 93:1171–1187

Moorthi S, Suarez MJ (1992) Relaxed Arakawa–Schubert—a parameterization of moist convection for general circulation models. Mon Weather Rev 120:978–1002

Neale RB, Richter JH, Jochum M (2008) The impact of convection on ENSO: from a delayed oscillator to a series of events. J Clim 21:5904–5924

Nordeng TE (1994) Extended versions of the convective parameterization scheme at ECMWF and their impact on the mean and transient activity of the model in the tropics. In: ECMWF research department, technical memorandum. ECMWF, reading No 206. October 1994, p 41

Pan HL, Wu WS (1995) Implementing a mass flux convection parameterization package for the NMC medium-range forecast model. NMC office note 409, p 40

Richter JH, Rasch PJ (2008) Effects of convective momentum transport on the atmospheric circulation in the Community Atmosphere Model, version 3. J Clim 21:1487–1499

Seo K-H, Son S-W (2012) The global atmospheric circulation response to tropical diabatic heating associated with the Madden-Julian oscillation during northern winter. J Atmos Sci 69:79–96

Seo K-H, Wang W (2010) The Madden-Julian oscillation simulated in the NCEP Climate Forecast System model: the importance of stratiform heating. J Clim 23:4770–4793

Seo K-H, Schemm JKE, Wang W, Kumar A (2007) The boreal summer intraseasonal oscillation simulated in the NCEP Climate Forecast System (CFS): the effect of sea surface temperature. Mon Weather Rev 135:1807–1827

Seo K-H, Lee H-J, Frierson DMW (2016) Unraveling the teleconnection mechanisms that induce wintertime temperature anomalies over the Northern Hemisphere continents in response to the Madden-Julian oscillation. J Atmos Sci 73:3557–3571

Sperber KR, Kim D (2012) Simplified metrics for the identification of the Madden-Julian oscillation in models. Atmos Sci Lett 13:187–193. doi:10.1002/asl.378

Thayer-Calder K, Randall DA (2009) The role of convective moistening in the Madden-Julian oscillation. J Atmos Sci 66:3297–3312

Tiedtke M (1989) A comprehensive mass flux scheme for cumulus parameterization in large-scale models. Mon Weather Rev 117:1779–1800

Waliser DE et al (2012) The "year" of tropical convection (May 2008–April 2010): climate variability and weather highlights. Bull Am Meteorol Soc 93:1189–1218

Wheeler MC, McBride JL (2011) Australian–Indonesian monsoon. In: Lau WKM, Waliser DE (eds) Intraseasonal variability in the atmosphere-ocean climate system, 2nd edn. Springer, New York, pp 147–198

Yoo C, Lee S, Feldstein SB (2012) Mechanisms of extratropical surface air temperature change in response to the Madden-Julian oscillation. J Clim 25:5777–5790

Yukimoto S et al (2011) Meteorological Research Institute Earth System Model Version 1 (MRI-ESM1): model description. Technical Report of the Meteorological Research Institute, No. 64, p 83

Zhang C (2005) Madden-Julian oscillation. Rev Geophys 43:RG2003. doi:10.1029/2004RG000158

Zhang GJ, McFarlane NA (1995) Sensitivity of climate simulations to the parameterization of cumulus convection in the Canadian Climate Centre general circulation model. Atmos Ocean 33:407–446

Zhang GJ, Mu M (2005) Effects of modifications to the Zhang-McFarlane convection parameterization on the simulation of the tropical precipitation in the National Center for Atmospheric Research Community Climate Model, version 3. J Geophys Res Atmos 110(D09):109

Zhang GJ, Wu X (2003) Convective momentum transport and perturbation pressure field from a cloud-resolving model simulation. J Atmos Sci 60:1120–1139

Zhao C, Li T, Zhou T (2013) Precursor signals and processes associated with MJO initiation over the tropical Indian Ocean. J Clim 26:291–307